RESEARCH ARTICLE

Human adipose tissue- and umbilical cord-derived stem cells: which is a better alternative to treat spinal cord injury?

Ai-Mei Liu[1], Bo-Li Chen[1], Ling-Tai Yu[1], Tao Liu[1], Ling-Ling Shi[1], Pan-Pan Yu[1], Yi-Bo Qu[1, 3], Kwok-Fai So[1, 2, 3, *], Li-Bing Zhou[1, 2, 3, *]

1 Guangdong-Hongkong-Macau Institute of CNS Regeneration, Ministry of Education CNS Regeneration Collaborative Joint Laboratory, Jinan University, Guangzhou, Guangdong Province, China

2 Guangzhou Regenerative Medicine and Health Guangdong Laboratory, Guangzhou, Guangdong Province, China

3 Co-innovation Center of Neuroregeneration, Nantong University, Nantong, Jiangsu Province, China

Funding: *This work was supported by Guangdong grant 'Key Technologies for Treatment of Brain Disorders', No. 2018B030332001 (to LBZ); Health and Medical Collaborative Innovation Major Projects of Guangzhou of China, Nos. 201803040016-2 (to LBZ), 201604046028 (to LBZ and KFS); Science & Technology Planning and Key Technology Innovation Projects of Guangdong Province of China, No. 2014B050504006 (to LBZ), Programme of Introducing Talents of Discipline to Universities of China, No. B14036 (to KFS), and Science and Technology Plan Project of Guangdong Province of China, No. 2017B090904033 (to KFS).*

Graphical Abstract

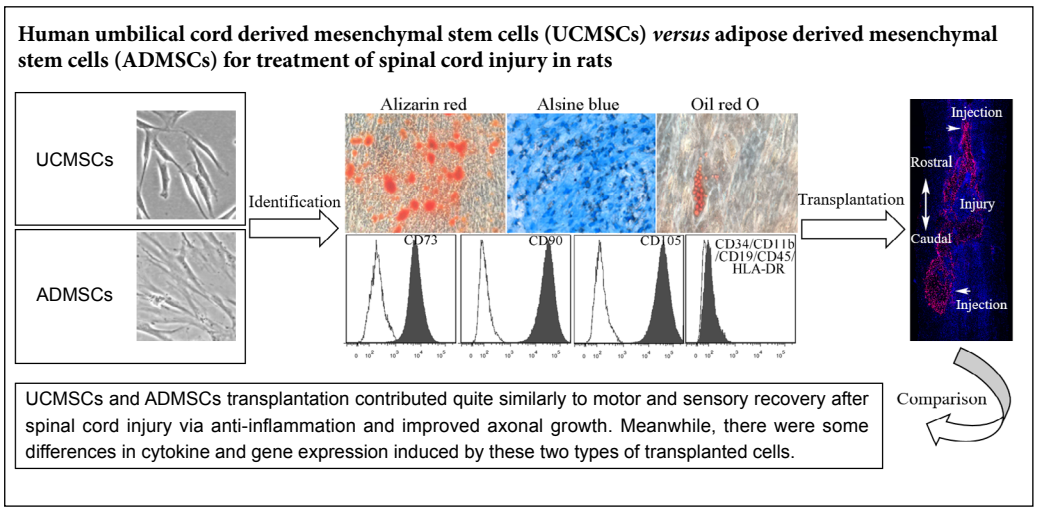

Correspondence to:
Li-Bing Zhou, PhD, tlibingzh@jnu.edu.cn;
Kwok-Fai So, PhD, hrmaskf@hku.hk.

orcid:
0000-0002-8975-5228 (Li-Bing Zhou)
0000-0003-4039-4246 (Kwok-Fai So)

doi: *10.4103/1673-5374.284997*

Received: *March 10, 2020*
Peer review started: *March 17, 2020*
Accepted: *April 3, 2020*
Published online: *June 19, 2020*

Abstract

Multiple types of stem cells have been proposed for the treatment of spinal cord injury, but their comparative information remains elusive. In this study, a rat model of T10 contusion spinal cord injury was established by the impactor method. Human umbilical cord-derived mesenchymal stem cells (UCMSCs) or human adipose tissue-derived mesenchymal stem cells (ADMSCs) (2.5 μL/injection site, 1×10^5 cells/μL) was injected on rostral and caudal of the injury segment on the ninth day after injury. Rats injected with mesenchymal stem cell culture medium were used as controls. Our results show that although transplanted UCMSCs and ADMSCs failed to differentiate into neurons or glial cells *in vivo*, both significantly improved motor and sensory function. After spinal cord injury, UCMSCs and ADMSCs similarly promoted spinal neuron survival and axonal regeneration, decreased glial scar and lesion cavity formation, and reduced numbers of active macrophages. Bio-Plex analysis of spinal samples showed a specific increase of interleukin-10 and decrease of tumor necrosis factor α in the ADMSC group, as well as a downregulation of macrophage inflammatory protein 3α in both UCMSC and ADMSC groups at 3 days after cell transplantation. Upregulation of interleukin-10 and interleukin-13 was observed in both UCMSC and ADMSC groups at 7 days after cell transplantation. Isobaric tagging for relative and absolute quantitation proteomics analyses showed that UCMSCs and ADMSCs induced changes of multiple genes related to axonal regeneration, neurotrophy, and cell apoptosis in common and specific manners. In conclusion, UCMSC and ADMSC transplants yielded quite similar contributions to motor and sensory recovery after spinal cord injury via anti-inflammation and improved axonal growth. However, there were some differences in cytokine and gene expression induced by these two types of transplanted cells. Animal experiments were approved by the Laboratory Animal Ethics Committee at Jinan University (approval No. 20180228026) on February 28, 2018, and the application of human stem cells was approved by the Medical Ethics Committee of Medical College of Jinan University of China (approval No. 2016041303) on April 13, 2016.

Key Words: *behavior; central nervous system; factor; inflammation; model; spinal cord; stem cells; transplantation*

Chinese Library Classification No. *R453; R365; R741*

Introduction

Spinal cord injury (SCI) disturbs spinal structure and neural networks, causing motor and sensory dysfunction. This poses a worldwide challenge (Jain et al., 2015; Kim and Ament, 2017), for which stem cell transplantation has become widely considered (Gazdic et al., 2018). Stem cells therapy raises issues in terms of cell sources, immune rejection, medical ethics, and safety and functional efficacy, which need to be considered prior to clinical applications.

Obtained from umbilical cord or bone marrow (Pittenger et al., 1999; Bianco et al., 2001), multipotent mesenchymal stem cells (MSCs) are accessible and have low tumorigenicity with few associated ethical restrictions (Bernardo et al., 2011; Munir and McGettrick, 2015; Vaquero et al., 2016; Matyas et al., 2017). Moreover, their immunomodulatory (Mukhamedshina et al., 2019) and neuroprotective properties (Amemori et al., 2010; Torres-Espín et al., 2013) are beneficial in SCI. For example, bone marrow-derived MSCs can reduce the production of proinflammatory factors tumor necrosis factor α (TNF-α) and interleukin (IL)-6, increase secretion of anti-inflammatory factors IL-4 and IL-13, promote M1 to M2 macrophage transformation, reduce axon and myelin loss, and inhibit glial scar formation (Nakajima et al., 2012). Adipose tissue-derived MSCs (ADMSCs) are an attractive source for cell therapy because they can be used in the future for autologous transplantation, have strong proliferation ability, are easy to culture, and generate few ethical problems (Hur et al., 2016; Fernandes et al., 2018). Human umbilical cord-derived MSCs (UCMSCs) also palliate limitations related to difficulties in generating sufficient cell numbers, and are thus an important cell source for transplantation (Secco et al., 2008; Han et al., 2013). MSCs derived from many different tissues have been compared in animal models of SCI. For example, compared with bone marrow-derived MSCs, transplantation of ADMSCs increased the expression of brain-derived neurotrophic factor and improved the microenvironment, which subsequently increased the retention of axons and reduced macrophage activation and cavity formation (Zhou et al., 2013). Moreover, the *in vitro* regenerative potential of UCMSCs and ADMSCs is not significantly different (Choudhery et al., 2013). However, whether UCMSCs and ADMSCs share similar or distinct contributions and mechanisms in SCI treatment remains largely unknown.

In this study, we compared the effects of UCMSCs and ADMSCs on functional improvements using a contusive rat SCI model. Our intention was to reveal putative mechanisms of UCMSCs and ADMSCs by applying multiplex cytokine immunoassay and isobaric tags for relative and absolute quantitation (iTRAQ)-based proteomics analysis.

Materials and Methods

Rat SCI model and cell transplantation

Animal experiments were approved by the Laboratory Animal Ethics Committee at Jinan University, China (approval No. 20180228026) on February 18, 2018. The application of human stem cells was approved by the Medical Ethics Committees of Medical College of Jinan University, China (approval No. 2016041303) on April 13, 2016, and was in accordance with the *Declaration of Helsinki*. A total of 150 adult female Sprague-Dawley rats aged 10 weeks and weighing 250 ± 25 g (Guangdong Medical Laboratory Animals Center, Guangdong, China; License No. SCXK (Yue) 2018-0002) underwent contusive SCI (Wu et al., 2017). Briefly, rats were anesthetized with 1.0–2.0% isoflurane (RWD, Shenzhen, China) and underwent laminectomy at the T10 level. The exposed dorsal surface of the T13 spinal segment was injured using a LISA impactor (Louisville Injury System Apparatus, Louisville, KY, USA) with a displacement of 1.0 mm for 0.5 seconds. After surgery, gentamicin (5 mg/kg; Guangdong Bangmin Pharmaceutical, Jiangmen, China) was administered for 3 days, and bladders were regularly emptied until animals urinated freely. Animals were selected for the transplantation protocol based on Basso, Beattie, and Bresnahan (BBB) scores (see below) measured for 2 consecutive days after surgery; animals with scores higher than 0 were excluded. SCI rats were randomly assigned to three groups that received UCMSCs (UCMSC group, n = 51), ADMSCs (ADMSC group, n = 51), or MSC culture medium (control group, n = 39) (Dulbecco's modified Eagle's medium-F12, 10% fetal bovine serum, 1% nonessential amino acids, and GlutaMAX; Thermo Fisher Scientific, Waltham, MA, USA) on the ninth day after injury. Protocols for MSC culture and identification are described in **Additional file 1**.

After opening the dura, cells (2.5 μL, 1×10^5 cells/μL for each injection) or an equal volume of culture medium were injected into two dorsomedial sites, rostral and caudal to the injury level. The total number of transplanted cells for each animal was about 5×10^5, corresponding to previous studies (Ruzicka et al., 2017; Khazaei et al., 2019). A microinjector (Cat. No. 1701; Hamilton, Bonaduz, Switzerland) was inserted at a depth of 1.6 mm and then withdrawn to 1.2 mm prior to injection. Injection was stopped for 10 seconds every 0.5 μL and the needle (glass electrode; Cat. No. 4878; World Precision Instruments, Sarasota, FL, USA) remained in position for 1 minute. Based on previous studies (Zhou et al., 2013; Salewski et al., 2015) and our preliminary tests, animals received cyclosporine A (15 mg/kg; Novartis, Basel, Switzerland) daily from two days before transplantation until the end of experiments to prevent immune rejection. Animals were maintained in environment-controlled rooms (22–24°C, 12-hour light/dark cycle).

Adeno-associated virus tracing

Six weeks after transplantation, adeno-associated virus 9 (AAV9)-green fluorescent protein (GFP) (0.25 μL, 1×10^{13} copies/mL; Vigene Biosciences Branch, Jinan, China) was injected into spinal cords at two segments rostral to the injury site. The injection depth was 1.2 mm below the parenchymal surface and the delivery speed was 0.2 μL/min. Two weeks after injection, animals (n = 6 per group) were fixed by perfusion and horizontal sections were prepared.

Behavioral tests

Locomotor hindlimb function was assessed by Basso, Beat-

tie, and Bresnahan scale (BBB) scores weekly after surgery for 8 weeks (n = 8 per group). CatWalk and footslip tests were performed weekly from 4–8 weeks after stem cell transplantation (n = 7 per group). Sensory function was measured using both von Frey and heat hyperalgesia tests weekly from 2–8 weeks after stem cell transplantation (n = 8 per group). Detailed protocols are described in **Additional file 2**.

Motor-evoked potential recordings

Fifty-six days after transplantation, motor-evoked potentials (MEPs) were recorded in the gastrocnemius muscle upon transcranial electrical stimulation in the motor cortex. Rats (n = 6 per group) were anesthetized with propofol (20 μL/g; Xi'an Libang Pharmaceutical, Xi'an, China) and immobilized in a stereotactic apparatus. After frontal skull exposure, the stimulating electrode was inserted into the motor cortex (M1) based on atlas coordinates. The recording electrode was placed in the contralateral gastrocnemius muscle, in a region which we were able to obtain stable recordings in control animals. After pulse stimulation (5000 mV, 0.2 ms at 1 Hz), recordings were made using a Keypoint Portable Electromyography Unit (Dantec Biomed, Skovlunde, Denmark) with a 30 Hz to 3 kHz bandpass filter.

Cytokine analysis

Three and 7 days after transplantation, 1-cm spinal segments surrounding injury sites were collected (n = 3 per group for each time point). Lysates were prepared in radioimmunoprecipitation assay buffer containing phenyl methane sulfonyl fluoride (1:100; Cat# P8340-1; Solarbio Bioscience and Technology, Beijing, China) and analyzed by Bio-Plex (Bio-Rad, Hercules, CA, USA) using a 23-Plex Cytokine Kit (Cat# 12005641, Bio-Rad) including anti-bodies against IL-1α, IL-1β, IL-2, IL-4, IL-5, IL-6, IL-7, IL-10, IL-12, IL-13, IL-17, IL-18, TNF-α, monocyte chemotactic protein 1, interferon-γ, macrophage inflammatory protein 1α, regulated upon activation normal T cell-expressed and -secreted factor, granulocyte colony-stimulating factor, C-X-C motif chemokine ligand 1, macrophage colony-stimulating factor, macrophage inflammatory protein 3α (MIP-3α), granulocyte-macrophage colony-stimulating factor, and vascular endothelial growth factor.

Proteomic analysis using iTRAQ

Spinal samples (1 cm long) centered on injury sites were collected seven days after transplantation (n = 3 per group). After protein extraction and concentration determination, 100 μg of each protein sample was reduced and alkylated, followed by enzymatic digestion and iTRAQ labeling according to the manufacturer's protocols (Applied Biosystems, Foster City, CA, USA). A Reagents 10-Plex Kit was used for UCMSC and ADMSC groups. Liquid chromatography–mass spectrometry (TripleTOF5600, Applied Biosystems) analysis was performed as previously described (Tang et al., 2018). Protein PilotTM (Version 4.5, Applied Biosystems) was used for protein identification and quantification. Criteria for differential protein expression were: coefficient of variation < 0.5, average ratio-fold change ≥ 1.5 or ≤ 0.67, and P value < 0.05 in the Student's t-test between groups.

Western blot assay

Results from iTRAQ were confirmed by western blots of the same samples used for iTRAQ, as previously described (Li et al., 2017). Proteins were incubated with primary antibodies overnight at 4°C, transferred to nitrocellulose membranes, and incubated for 1 hour at room temperature with secondary antibodies. Primary antibodies are summarized in **Additional Table 1**. Secondary antibodies included horseradish peroxidase-conjugated goat anti-rabbit IgG (1:5000; Cat# ab6721; Abcam, Cambridge, UK), donkey anti-goat IgG (1:5000; Cat# ab6885; Abcam), and goat anti-mouse IgG (1:5000; Cat# ab6789; Abcam). Signal was evaluated using a luminescent kit (Cat# WBKLS0100; Millipore, Bedford, MA, USA), and quantified using ImageJ software (National Institutes of Health, Bethesda, MD, USA). Experiments were carried out at least in triplicate.

Immunofluorescence staining

Rats were perfused with 4% paraformaldehyde (Solarbio Bioscience and Technology), and spinal segments (about 1 cm around the injury center) were dissected and stored in the same fixative. Serial transverse or horizontal sections (20-μm thick) were prepared with a cryostat for immunofluorescence staining. Sections were incubated with primary antibodies overnight at 4°C, followed by secondary antibodies for 1 hour at room temperature. Primary antibodies are listed in **Additional Table 1**. Signal was evaluated as the fluorescence of Alexa Fluor 488- or 546-conjugated secondary antibodies (1:1000; Cat# A21202/A10040/A31571; Thermo Fisher Scientific).

Image analysis

Images were captured with a fluorescence confocal microscope (LSM700; Zeiss, Oberkochen, Germany) and analyzed using ImageJ. In each spinal block, ten series of transverse sections or five series of horizontal sections were prepared for single, double, or triple immunostaining. In each series, the spacing of two adjacent sections was 200 μm (transverse sections) or 100 μm (horizontal sections). All stained sections were used for analysis.

Transplanted cell survival and differentiation

Transverse sections were immunostained for anti-human nuclear antibody (HUNA), and total HUNA-positive cells were counted using the Abercrombie formula (Abercrombie, 1946) at 7, 14, 21, and 28 days after stem cell transplantation. Survival rates were calculated as the ratio of HUNA-positive cells to the total number of transplanted cells. Similarly, spinal sections were double-labeled for HUNA and βIII-tubulin (TUJ1), glial fibrillary acidic protein (GFAP), paired box 6 (PAX6), or oligodendrocyte transcription factor 2 (Olig2) at 14 days after stem cell transplantation. For each timepoint, six animals from each group were evaluated.

Cell densities

In each section, ionized calcium-binding adapter molecule 1

(Iba1)-positive cells were counted in three randomly chosen fields (0.5 mm × 0.5 mm) of dorsal areas using ImageJ; cell densities were extrapolated. Spinal levels at a distance of 4 mm from the injury site were evaluated 56 days after stem cells transplantation. NeuN-positive and choline acetyltransferase (ChAT)-positive neurons were also counted 56 days after stem cell transplantation using ImageJ. Six animals from each group were evaluated.

Fiber density

Horizontal spinal cord sections (about 12–15 sections), including the lesion area, were prepared 56 days after stem cells transplantation. In each section, parallel horizontal lines were defined at different distances from the injury center, and the number of fibers positive for neurofilament 200 (NF200)- and AAV9-GFP-positive that intercepted each line was counted (length > 40 μm), as previously described (Anderson et al., 2018). Average intercepts per section were measured in six animals from each group.

Evaluation of glial scar and lesion cavity volumes

Glial scars and lesion cavities were quantified by three-dimensional (3D) reconstruction of serial transverse sections stained for GFAP at 56 days after stem cells transplantation. Ten serial transverse spinal sections equally spaced by 200 μm were used to create a 3D image corresponding to a 1 cm-long spinal cord segment. Neurolucida (MBF Bioscience, Williston, VT, USA) was used to calculate glial scar and lesion cavity volumes (Sun et al., 2018). Five animals from each group were evaluated.

Myelin basic protein immunofluorescence density

Images of entire transverse sections stained for myelin basic protein (MBP) 56 days after stem cells transplantation were captured with consistent exposure time under the same conditions with a 20× objective using Zen tiling (imager Z2 Zeiss). Immunoreactive density was measured using ImageJ. Six animals from each group were imaged.

Magnetic resonance imaging

Eight weeks after transplantation, magnetic resonance imaging (MRI) was performed with a 9.4T small-bore scanner (Bruker Biospec, Ettlingen, Germany) and single-channel surface coil (20-mm diameter). Rats (n = 5 per group) were anesthetized with 1.0–2.0% isoflurane and immobilized with a custom head positioner, heating equipment, breathing and temperature monitor, and electrocardiogram probe. Sagittal and axial T2-weighted images and diffusion tensor imaging (DTI) were obtained. DTI imaging was performed using echo planar imaging-DTI sequences with electrocardiogram-gated standard diffusion.

Statistical analysis

Data are presented as the mean ± standard error of the mean (SEM). Comparisons among different time points or distances in the two or three groups were performed using two-way repeated measures analysis of variance with Bonferroni's *post-hoc* correction. Other data were analyzed using one-way analysis of variance with Tukey's multiple comparison test or Student's *t*-test (Prism 7.0, GraphPad, San Diego, CA, USA). The significant difference level was set to 0.05.

Results

Transplanted UCMSCs and ADMSCs show similar characteristics *in vivo*

UCMSCs and ADMSCs, which maintained MSC properties and high purity *in vitro* (**Additional Figure 1**), were transplanted 9 days after SCI. Spinal samples were collected at various time points after transplantation. Anti-HUNA immunostaining showed that transplanted UCMSCs and ADMSCs migrated longitudinally and accumulated around injury sites by 14 days (**Figure 1A** and **B**). To assess the survival of transplanted cells, we prepared sections at different time points and carried out anti-HUNA immunostaining. Many HUNA-positive UCMSCs and ADMSCs were visible on days 7, 14, and 21 (**Figure 1A1**–**A3** and **B1**–**B3**). However, on day 21, HUNA-labeled nuclei became round and condensed, indicating poor cell condition, and only a small number of HUNA-positive cells were visible on day 28 in both UCMSC and ADMSC groups (**Figure 1A3**, **B3**, **A4**, and **B4**). Quantification indicated no significant differences in survival rates of UCMSCs and ADMSCs at any time point (P > 0.05 at days 7, 14, 21, and 28; **Figure 1C**).

As significant numbers of transplanted cells survived until 14 days after transplantation, we carried out double immunostaining to assess their differentiation *in vivo*. Anti-HUNA and PAX6 immunostaining showed that HUNA-positive cells were negative for PAX6 in UCMSC and ADMSC groups (**Figure 2A**, **A'**, **C**, and **C'**). Interestingly, some PAX6-positive cells were present around HUNA-positive cells, indicating that transplanted UCMSCs and ADMSCs probably induced endogenous cell proliferation. Few HUNA-positive cells co-expressed TUJ1, Olig2, or GFAP (**Figure 2B**–**H** and **B'**–**H'**), indicating that transplanted UCMSCs or ADMSCs failed to differentiate into neurons or glia cells without specific induction *in vivo*.

Transplanted cells contribute to functional recovery from SCI

To estimate the contribution of transplanted cells in functional recovery after SCI, we performed a moderate contusion in rats at T10 and monitored their recovery of hindlimb movement using BBB scores (Bhimani et al., 2017). All animals had complete hindlimb paralysis with a BBB score of 0 at 1 day after injury and underwent spontaneous recovery thereafter (**Figure 3A**). To avoid the peak of inflammation in spinal cords, we transplanted cells 9 days after injury. BBB scores increased progressively and reached a plateau at 28 days post-transplantation in UCMSC and ADMSC groups (**Figure 3A**). At 28, 42, 49, and 56 days, BBB scores were significantly higher in UCMSC and ADMSC groups compared with the control group (UCMSC *vs.* control: P < 0.05 at 28, 42, 49, and 56 days; ADMSC *vs.* control: P < 0.05 at 28 and 42 days, P < 0.01 at 49 and 56 days), but were not significant-

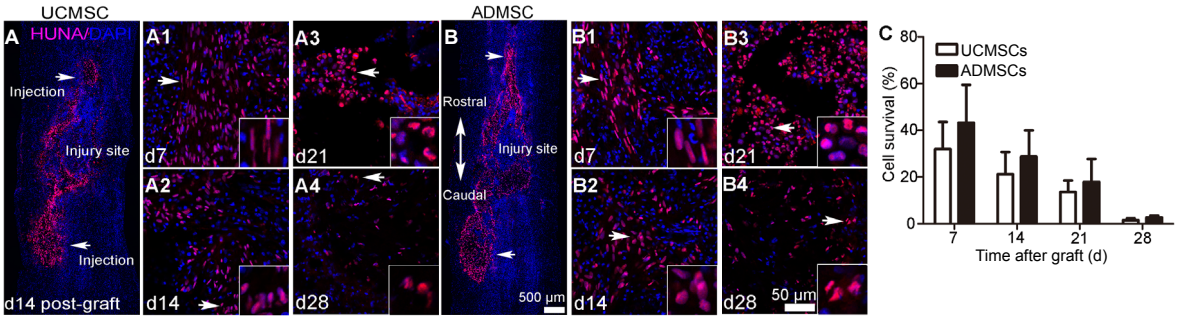

Figure 1 Migration and survival of transplanted cells *in vivo*.
(A, B) Horizontal spinal cord sections spanning injury sites were immunostained for HUNA at 14 days (d14) after UCMSC (A) or ADMSC (B) transplantation. HUNA-positive cells migrated longitudinally from the injection site (arrows) and accumulated around the injury site. (A1–4, B1–4) Transverse sections were immunostained for HUNA at d7 (A1, B1), d14 (A2, B2), d21 (A3, B3), and d28 (A4, B4) after UCMSC (A1–4) or ADMSC (B1–4) transplantation. In both groups, a large number of HUNA-positive cells were visible from d7 to d21, but only a few remained at d28. By d21, HUNA-labeled nuclei became round and shrunken in contrast to the observed long-spindle shapes at d7 and d14 (insets). Square boxes in A1–A4 and B1–B4 show high magnification of selected regions (arrows) in corresponding images. HUNA (red): Alexa Fluor 546. All sections were stained with DAPI (blue). Scale bars: 500 μm in A, B; 50 μm in A1–B4. (C) Survival of transplanted UCMSCs and ADMSCs. Numbers of transplanted UCMSCs and ADMSCs gradually decreased with time, and only a few cells survived by d28 after transplantation. No significant difference was observed between the two groups. Data are presented as the mean ± SEM (n = 6 per group for each time point), and analyzed by two-way repeated measures analysis of variance with Bonferroni's *post hoc* correction. ADMSCs: Adipose-derived mesenchymal stem cells; DAPI: 4′,6-diamidino-2-phenylindole; HUNA: human nuclear antibody; UCMSCs: umbilical cord-derived mesenchymal stem cells.

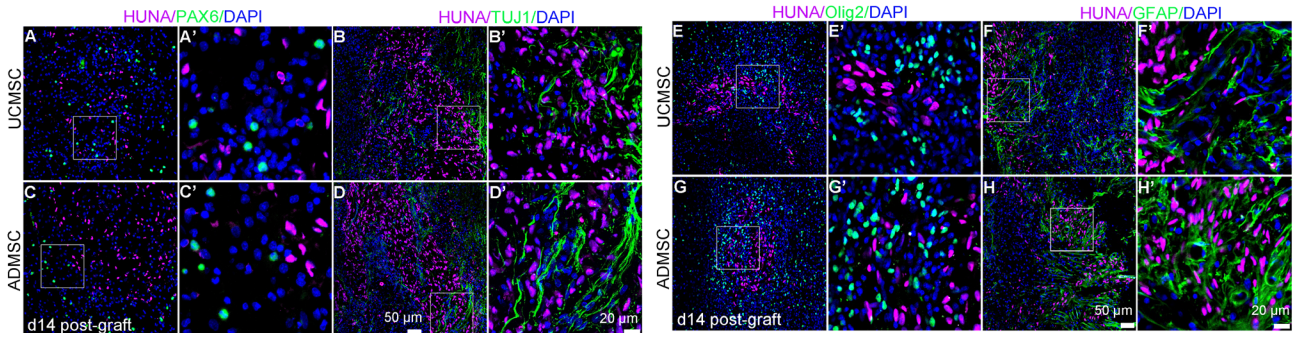

Figure 2 Few transplanted UCMSCs or ADMSCs differentiate into neurons or glial cells *in vivo*.
(A–H) Fourteen days (d14) after UCMSC (A, B, E, F) or ADMSC (C, D, G, H) transplantation, spinal sections were processed with double immunofluorescence staining for HUNA and PAX6 (A, C), TUJ1 (B, D), Olig2 (E, G), or GFAP (F, H). (A'–H') All HUNA-positive cells were negative for PAX6 (A', C'), TUJ1 (B', D'), Olig2 (E', G'), and GFAP (F', H'). After UCMSC or ADMSC transplantation, PAX6-positive cells (negative for HUNA) surrounded transplanted UCMSCs (A) and ADMSCs (C). A'–H' are boxed regions from A–H. n = 6 per group. HUNA (violet): Alexa Fluor 546; PAX6 (green), TUJ1 (green), Olig2 (green), GFAP (green): Alexa Fluor 488. All sections were stained with DAPI (blue). Scale bars: 50 μm in A–H; 20 μm in A'–H'. ADMSCs: Adipose-derived mesenchymal stem cells; DAPI: 4′,6-diamidino-2-phenylindole; GFAP: glial fibrillary acidic protein; HUNA: human nuclear antibody; Olig2: oligodendrocyte transcription factor 2; PAX6: paired box 6; TUJ1: βIII-tubulin; UCMSCs: umbilical cord-derived mesenchymal stem cells.

ly different between UCMSC and ADMSC groups (P > 0.05; **Figure 3A**).

To further assess locomotion improvement, we performed CatWalk tests at 28, 35, 42, 49, and 56 days after transplantation. Numbers of defective hindlimb steps were significantly decreased and the Regularity Index was significantly increased compared with control animals (UCMSC *vs.* control: P < 0.01 at 28 days, P < 0.05 at 35, 42, and 56 days; ADMSC *vs.* control: P < 0.01 at 28 and 56 days, P < 0.05 at 35 and 49 days), with no differences between UCMSC and ADMSC groups (P > 0.05; **Figure 3B**). Similarly, maximal hindpaw contact areas were significantly higher in UCMSC and ADMSC groups compared with the control group (UCMSC *vs.* control: P < 0.01 at 35 days, P < 0.05 at 42, 49, and 56 days; ADMSC *vs.* control: P < 0.05 at 28, 42, 49, and 56 days, P < 0.001 at 35 days), but comparable between UCMSC and ADMSC groups (P > 0.05; **Figure 3C**).

In the grid test, numbers of footslips were significantly decreased in UCMSC and ADMSC groups compared with the control group (UCMSC *vs.* control: P < 0.01 at 49 days, P < 0.05 at 56 days; ADMSC *vs.* control: P < 0.05 at 35, 42, 49, and 56 days), but comparable between UCMSC and ADMSC groups (P > 0.05; **Figure 3D**).

To provide electrophysiological evidence of motor recovery, we recorded MEPs at 56 days after transplantation by recording electromyographic activity of the gastrocnemius muscle upon stimulation of the motor cortex (Yang et al., 2015) (**Figure 3E**). MEP amplitudes observed in UCMSC and ADMSC groups were significantly higher than those observed in control animals (UCMSC or ADMSC *vs.* control: P < 0.05, P < 0.01; UCMSC *vs.* ADMSC: P > 0.05; **Figure 3F**).

To evaluate sensory function at different time points after transplantation, we estimated mechanical allodynia using the von Frey test and thermal hyperalgesia after laser stimulation. Compared with controls, thresholds of hindpaw withdrawal were significantly increased in UCMSC and ADMSC groups (UCMSC *vs.* control: P < 0.05 at 14 and 42 days, P < 0.001 at 21 days; ADMSC *vs.* control: P < 0.01 at 21 days, P < 0.05 at 42 and 56 days; UCMSC *vs.* ADMSC: P > 0.05; **Figure 3G**). Similar changes were observed in hyperalgesia tests,

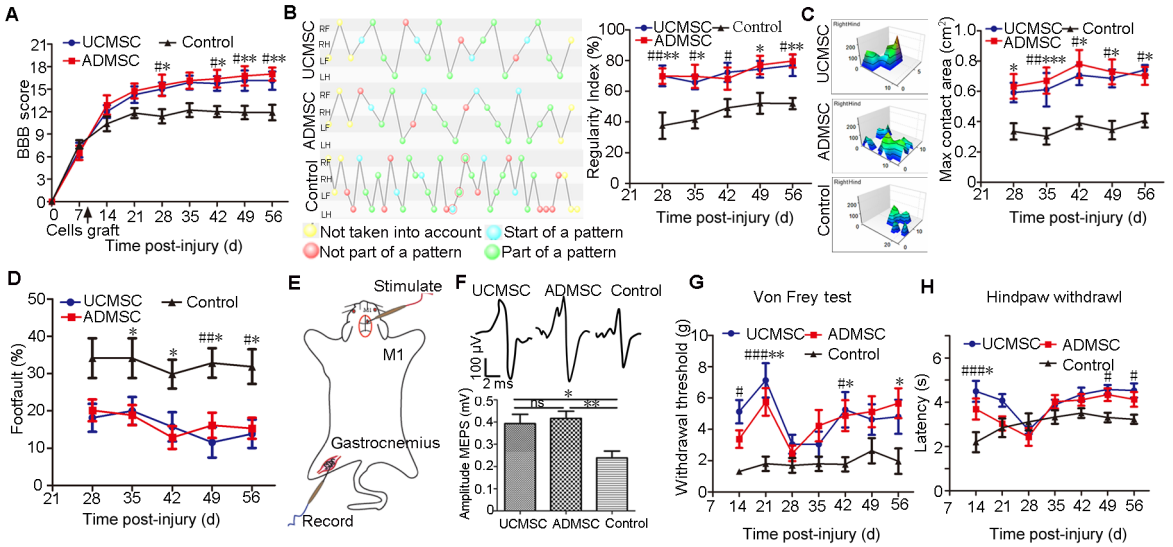

Figure 3 Transplanted UCMSCs and ADMSCs similarly improve motor and sensory function.
(A) BBB scores evaluated for 8 consecutive weeks after SCI. In UCMSC and ADMSC groups, there was no significant difference during the first 3 weeks, and a significant increase from the fourth to eighth weeks, compared with the control group (n = 8 per group). BBB scores were comparable in UCMSC and ADMSC groups at all time points. The arrow on the abscissa indicates time of transplantation. (B, C) Locomotor evaluation using the CatWalk test from the fourth to eighth weeks after transplantation (n = 7 per group). (B) A significant increase of Regularity Index was oberved in UCMSC and ADMSC groups at each time point compared with the control group. (C) The maximum hindpaw contact area was increased in UCMSC and ADMSC groups compared with the control group. Yellow dots: Not taken into account; blue dots: start gaits; green dots: normal gaits; red dots: wrong gaits. (D) Footslip testing was performed weekly from the fourth to eighth weeks after transplantation (n = 7 per group). A similarly significant decrease in the number of footslips was observed in UCMSC and ADMSC groups compared with the control group. (E, F) MEP recordings 8 weeks after transplantation, with stimulation in motor cortex and recording in gastrocnemius muscle (E). MEP amplitudes were significantly increased in UCMSC and ADMSC groups (F) compared with the control group (n = 6 per group). (G, H) Mechanical (G) and thermal (H) sensitivity assessed from the second to eighth weeks after transplantation (n = 8 per group). (G) Von Frey test showed a significant increase of withdrawal threshold in UCMSC and ADMSC groups. (H) Latencies of hindpaw withdrawal were increased in UCMSC and ADMSC groups compared with the control group. Data are presented as mean ± SEM. #P < 0.05, ##P < 0.01, ###P < 0.001, UCMSC group *vs.* control group; *P < 0.05, **P < 0.01, ***P < 0.001, ADMSC group *vs.* control group. F shows one-way analysis of variance with Tukey's multiple comparison test; other panels show two-way repeated measures analysis of variance with Bonferroni's *post hoc* correction. ADMSC: Adipose-derived mesenchymal stem cell; BBB: Basso, Beattie and Bresnahan scale; M1: motor cortex; MEP: motor-evoked potential; ns: not significant; SCI: spinal cord injury; UCMSC: umbilical cord-derived mesenchymal stem cell.

with increased latencies in UCMSC and ADMSC groups (UCMSC *vs.* control: P < 0.001 at day 14, P < 0.05 at days 49 and 56; ADMSC *vs.* control: P < 0.05 at day 14; UCMSC *vs.* ADMSC: P > 0.05; **Figure 3H**).

Transplanted cells influence glial scar formation and reduced lesion size

After SCI, transplanted MSCs may modulate neuroinflammation and glial scar formation (Nakajima et al., 2012). To assess this, live animals were examined with MRI to acquire T2-weighted images and DTI about 2 months after transplantation (**Figure 4A**). Fibers spanning injured regions looked better preserved in UCMSC and ADMSC groups compared with the control group (**Figure 4B**). Fractional anisotropy values, which are positively correlated with axonal density (Lehmann et al., 2010), were significantly increased at +3 mm rostral to the injury center in UCMSC and ADMSC groups (UCMSC *vs.* control: P < 0.05; ADMSC *vs.* control: P < 0.05), and at –3 mm caudal to the injury center in the ADMSC group (ADMSC *vs.* control: P < 0.05; **Figure 4C**). Radial diffusivity values, which reflect axonal demyelination after injury (Aung et al., 2013), were significantly decreased in UCMSC and ADMSC groups at +2 mm (UCMSC or ADMSC *vs.* control: P < 0.05), +1 mm (UCMSC *vs.* control: P < 0.05; ADMSC *vs.* control: P < 0.01), and –1 mm (UCMSC or ADMSC *vs.* control: P < 0.05) compared with the control group (**Figure 4D**). Statistical analysis of reconstructed images revealed reduced lesion area in UCMSC and ADMSC groups compared with the control group at +1 mm, 0 mm, and –1 mm from the epicenter (UCMSC *vs.* control: P < 0.05, P < 0.01, and P < 0.05 at 1, 0, and –1 mm, respectively; ADMSC *vs.* control: P < 0.01, P < 0.01, and P < 0.05 at 1, 0, and –1 mm, respectively; UCMSC *vs.* ADMSC: P > 0.05 at 1 mm, 0 mm, and –1 mm, respectively; **Figure 4E**).

To confirm these results, we stained serial transverse sections collected 56 days after transplantation with a GFAP antibody (**Figure 5A**), and prepared 3D reconstructions using Imaris microscopy image analysis software (Oxford Instruments, Zurich, Switzerland) (**Figure 5B**). The glial scar and cavity were well defined, and their size decreased gradually from the epicenter to rostral and caudal levels in all groups (**Figure 5A**). We measured the volume of GFAP-positive glial scar and lesion cavity, and expressed this relative to spinal volume. Our results indicated significant reductions in glial scar and lesion cavity volumes in UCMSC and ADMSC groups compared with the control group [UCMSC or ADMSC *vs.* control: P < 0.05 (glial scar); UCMSC or ADMSC *vs.* control: P < 0.05 or P < 0.01 (lesion cavity)], with no difference between UCMSC and ADMSC groups (P > 0.05; **Figure 5C** and **D**).

UCMSCs and ADMSCs contribute to spinal neuron survival and slow axonal demyelination and degeneration

To evaluate the effect of transplanted cells on neuron survival, we performed anti-NeuN immunostaining for total spinal neurons and anti-ChAT immunostaining for spinal motor neurons in serial sections from 4 mm caudal to 4 mm rostral of the injury center 56 days after transplantation. NeuN-labeled cells were rarely identified in the injury center and gradually increased with distance from the center, caudally and rostrally, in all groups (**Additional Figure 2C**). Numbers of NeuN-positive neurons were significantly higher in UCMSC and ADMSC groups compared with the control group, particularly at +4, –3, and –4 mm sites in the UCMSC group (UCMSC *vs*. control: $P < 0.05$ at 4 mm and –4 mm; $P < 0.01$ at –3 mm) and ADMSC group (ADMSC *vs.* control: $P < 0.05$ at –3 mm; $P < 0.01$ at –4 mm; **Additional Figure 2C**). Double immunostaining for NeuN and ChAT revealed that some spinal motor neurons survived away from the epicenter (**Additional Figure 2B**), as more ChAT-positive neurons were observed farther from the epicenter caudally and rostrally. Compared with the control, numbers of motor neurons were significantly higher at +4 mm and +3 mm rostral to the injury epicenter in the UCMSC group ($P < 0.05$), and +4, +3, –3, and –4 mm away from the epicenter in the ADMSC group ($P < 0.05$; **Additional Figure 2D**). These results suggest that transplanted UCMSCs and ADMSCs promoted spinal neuron survival, and there was no significant difference between UCMSC and ADMSC groups ($P > 0.05$; **Additional Figure 2C** and **D**).

Axonal degeneration and demyelination were monitored using MRI, which indicated that fibers and myelin were better preserved after UCMSC or ADMSC transplantation (as indicated by fractional anisotropy and radial diffusivity values shown in **Figure 4**). To confirm this, we prepared serial transverse sections surrounding lesions and carried out immunostaining for MBP and NF200 at 56 days post-transplantation; in addition, we performed AAV9-GFP labeling at 42 days. Anti-NF200 staining revealed the preservation of some fibers around injury sites in all groups (**Figure 6A**). At the injury center, axonal profiles were significantly more abundant in UCMSC and ADMSC groups compared with the control group (UCMSC or ADMSC *vs*. control: $P < 0.05$ or $P < 0.01$), with no differences between UCMSC and ADMSC groups ($P > 0.05$; **Figure 6B**). In all groups, AAV9-GFP injection rostral to the injury site labeled sparse fibers crossing the lesioned area to caudal regions, where more labeled axons were observed compared with the injury epicenter (**Figure 6C**), indicating that some axons sprouted and/or regenerated from spared fibers. Quantification confirmed a significant increase of AAV9-GFP-labeled fibers at –3 mm in UCMSC and ADMSC groups (UCMSC *vs*. control: $P < 0.05$; ADMSC *vs*. control: $P < 0.01$; **Figure 6D**). However, no significant difference was observed between UCMSC and ADMSC groups ($P > 0.05$; **Figure 6D**).

In UCMSC and ADMSC groups, MBP expression was stronger than observed in the control (**Additional Figure 3**), with significant increases at +2, +1, and -2 mm from the injury epicenter in the UCMSC group (UCMSC *vs*. control (average density): $P < 0.05$), and +2, +1, –1, –2, and –3 mm from the epicenter in the ADMSC group (ADMSC *vs*. control: $P < 0.05$). There was no significant difference between UCMSC and ADMSC groups ($P > 0.05$; **Additional Figure 3B**).

UCMSCs and ADMSCs alleviate neuroinflammation

Inflammatory cytokines mediate secondary injury after SCI. To assess whether transplanted cells influenced cytokine production, cytokine levels were measured in spinal samples from injury sites 3 and 7 days after transplantation (**Figure 7A** and **Additional Figure 4**). Compared with controls at 3 days after transplantation, upregulation of the anti-inflammatory factor IL-10 and downregulation of the proinflammatory TNF-α occurred in the ADMSC group (ADMSC *vs*. control: $P < 0.05$, $P < 0.01$); whereas, downregulation of pro-inflammatory MIP-3α was observed in both UCMSC and ADMSC groups (UCMSC or ADMSC *vs*. control: $P < 0.05$; **Figure 7B**). Furthermore, anti-inflammatory factors IL-10 and IL-13 were significantly increased in UCMSC and ADMSC groups 7 days after transplantation (UCMSC or ADMSC *vs.* control: $P < 0.05$ for IL-10 or IL-13; **Figure 7B**), indicating that both UCMSCs and ADMSCs alleviated neuroinflammation. However, ADMSCs better promoted anti-inflammatory factor expression and inhibited pro-inflammatory factor expression compared with UCMSCs during the early period.

After SCI, the activation status of microglial cells serves as an indicator of neuroinflammation (Hausmann, 2003). We examined microglial cells at 56 days after transplantation with Iba1 immunostaining. At 4 mm rostral to the injury site, most microglial cells exhibited a sting-state morphology (star-shaped with multiple branches) in UCMSC and ADMSC groups, whereas an active phenotype (round soma with few branches) was observed in the control (**Figure 7C**). Furthermore, Iba1-positive cells were less abundant in UCMSC and ADMSC groups compared with the control group (UCMSC *vs*. control: $P < 0.05$; ADMSC *vs.* control: $P < 0.01$; **Figure 7D**). There was no significant difference in microglial activation states between UCMSC and ADMSC groups ($P > 0.05$; **Figure 7D**).

Transplanted cells induce proteomic changes

To further explore potential molecular mechanisms, we used iTRAQ to estimate levels of proteins extracted from 1-cm spinal segments around the injury site 7 days after transplantation. Expression of multiple proteins related to axonal regeneration was significantly modified in UCMSC and ADMSC groups, including fasciculation and elongation protein zeta-1 (FEZ1), transportin 1 (TNPO), serine/threonine-protein kinase (DCLK2), canopy 2 homolog (Zebrafish) (CNPY2), complexin-1 (CPLX1), and signal transducer and activator of transcription 3 (STAT3) (**Additional Figure 5**). In addition, expression of unconventional myosin-1b (MYO1B), cathepsin B (CATB), receptor-type tyrosine-protein phosphatase F (PTPRF), cell division control protein

42 homolog (CDC42), zinc transporter 3 (SLC30A3), and growth associated protein-43 (GAP43) were specifically modified in the UCMSC group (**Additional Figure 5**). In the ADMSC group, expression of collagen alpha-2(I) chain (COL1A2), coronin-2B (CORO2B), vasodilator-stimulated phosphoprotein (VASP), coronin-1A (CORO1A), and coronin-1C (CORO1C) underwent specific changes (**Additional Figure 5**). To confirm iTRAQ results, we performed western blotting with antibodies against GAP43, CATB, and CDC42, which were confirmed to be specifically upregulated in the UCMSC group, but not the ADMSC group (**Figure 8A**). In addition, western blot results confirmed the upregulation of CORO1A and downregulation of COL1A2 in the ADMSC, but not the UCMSC group (**Figure 8B**). Moreover, upregulation of STAT3 (total and phosphorylated) and CNPY2 was confirmed in both UCMSC and ADMSC groups (**Figure 8C**).

Discussion

Increasing evidence indicates that stem cell transplantation is a promising therapy for SCI (Dalamagkas et al., 2018; DeBrot and Yao, 2018). Several types of cells have been evaluated in animal models and a few are being tested in clinical trials. The question of which cell type to use is critical, and requires comparative evaluations in animal models under controlled conditions. To provide some basic information for clinical trials, we report our comparison of two human-derived stem cell sources for the treatment of SCI, using a subacute moderate injury rat model. Our results indicate that UCMSCs and ADMSCs are equally effective and beneficial under the same conditions (summarized in **Additional Table 2**).

After SCI, primary and secondary injuries result in neuronal loss, interruption of neural networks, and functional deficits. Ideally, transplanted cells should help replace lost neurons, reduce secondary injury, slow cell death and axonal demyelination, promote axonal regeneration and neural plasticity, and restore function. UCMSCs and ADMSCs partially fulfilled some of those objectives. Comparable beneficial effects of UCMSCs and ADMSCs are supported by the following evidence: (i) a fraction of transplanted cells survived after transplantation and migrated towards the injury site; (ii) after transplantation, lesion cavities and glial scar volumes were decreased, as assessed by 3D reconstruction and MRI; (iii) UCMSC or ADMSC transplantation significantly slowed down neuronal death in regions adjacent to the injury epicenter, and increased the preservation of total and motor neurons; (iv) after transplantation, axonal fibers were better preserved, as indicated by a significant increase of NF200 positivity, AAV tracing, and MRI; (v) UCMSCs and ADMSCs probably induced endogenous cell proliferation, as indicated by observations of PAX6-positive cells around transplanted cells; and (vi) UCMSCs and ADMSCs promoted motor and sensory recovery, as assessed by BBB scores, CatWalk test, grid walking, MEP recording, von Frey filament test, and thermal test.

Notably, transplanted UCMSCs and ADMSCs did not differentiate into neurons or glial cells, indicating that they cannot replace lost neurons *in vivo*. Although UCMSCs and ADMSCs can be reprogrammed into neuron-like cells (Chen et al., 2016; Gao et al., 2019), this requires the activity of factors such as sonic hedgehog and retinoic acid, whose risk to patients might not be negligible and thus needs more evaluation. In our samples, PAX6-positive, HUNA-negative cells surrounded HUNA-positive UCMSCs or ADMSCs, suggesting that transplanted cells may activate endogenous cell proliferation, thus contributing to neural plasticity (Yang et al., 2015; Zhang et al., 2019). Another issue for clinical applications concerns the survival of transplanted cells. In our study, most UCMSCs and ADMSCs died 4 weeks after transplantation, and it remains to be seen whether successive transplantations or increased numbers of transplanted cells could further improve functional recovery. After SCI, proliferating astrocytes form a glial scar that hampers axonal growth (Orlandin et al., 2017). Both UCMSCs and ADMSCs limited glial scar formation, thereby providing favorable conditions for regrowth of spared axons across the injury site. Our finding of increased numbers of axonal fibers after UCMSC or ADMSC transplantation may result from decreased axonal degeneration and/or increased axonal sprouting.

Our Bio-Plex immunoassay results show that both UCMSCs and ADMSCs alleviated local neuroinflammation, promoted the secretion of beneficial cytokines, and inhibited microglia activation and proliferation around the injury site. Of potential interest is the observation of downregulated expression of pro-inflammatory cytokines TNF-α and MIP-3α, which was accompanied by upregulation of anti-inflammatory cytokines IL-10 and IL-13 early after transplantation. TNF-α contributes to neuronal apoptosis as part of the secondary injury after SCI, and inhibition of TNF-α signaling contributes to recovery (Wang et al., 2014). IL-10 and IL-13 contribute to tissue sparing, neuronal survival, and functional and histopathological recovery after SCI (Thompson et al., 2013; Dooley et al., 2016). Some differences between UCMSCs and ADMSCs, especially ADMSC-specific upregulation of IL-10 and downregulation of TNF-α, may indicate an advantage of ADMSCs over UCMSCs in controlling neuroinflammation.

Results of our iTRAQ screen show that both UCMSCs and ADMSCs activate expression of endogenous genes that promote neural plasticity and axonal sprouting. Notably, transplantation increased expression of FEZ1, DCLK2, CNPY2 and STAT3, which promote neurite growth (Grant et al., 1992; Bornhauser et al., 2003; Kang et al., 2011; Shin et al., 2013; Mehta et al., 2016). In addition, expression of some proteins was differentially modified upon UCMSC versus ADMSC transplantation. Significant increases of GAP43, CATB, and CDC42, all of which contribute to axonal growth (Pertz et al., 2008; Grasselli and Strata, 2013; Tran et al., 2018), were observed in the UCMSC group, contrary to the ADMSC group. However, changes in CORO1C, CORO2B, and CORO1A, which have neurotrophic actions (Suo et al., 2014), were present in the ADMSC group, but not the UCMSC group. Therefore, UCMSCs and ADMSCs may exert

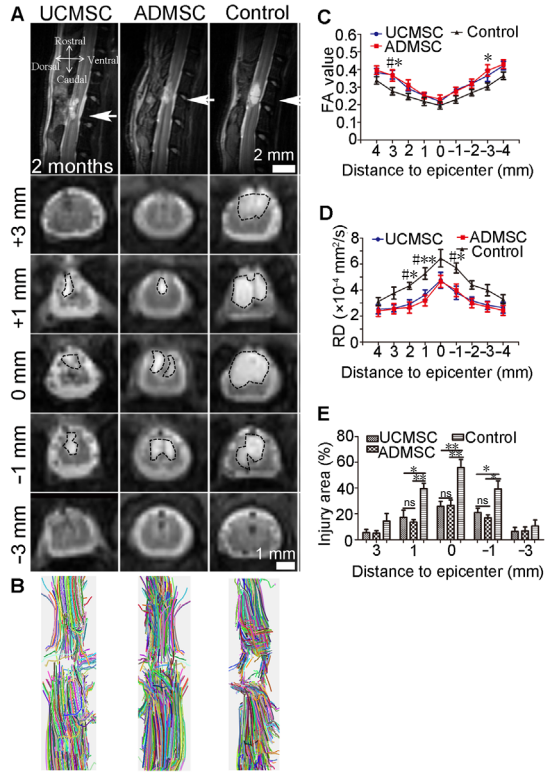

Figure 4 MRI of live animals with spinal cord injury after UCMSC or ADMSC transplantation.

(A) Sagittal and transverse sections spanning from –3 mm caudal to +3 mm rostral from the injury epicenter (arrows) 2 months after UCMSC or ADMSC transplantation, or in the control group. Lesion areas are outlined in black. Scale bar: 2 mm (sagittal); 1 mm (transverse). (B) Examples of colored fiber tractography images of the injured spinal cord reconstructed by diffusion tensor imaging. There were more crossing fibers at the injury site in UCMSC and ADMSC groups than in the control group. (C–E) In UCMSC and ADMSC groups, there was a significant increase of FA values (C), as well as a significant decrease of RD values (D) and injury areas (E) compared with the control group. Data are presented as mean ± SEM (n = 5 per group). Two-way repeated measures analysis of variance with Bonferroni's *post-hoc* correction in C–E. In C and D: #P < 0.05, comparison between UCMSC and control groups; *P < 0.05 and **P < 0.01, comparison between ADMSC and control groups. ADMSC: Adipose-derived mesenchymal stem cell; FA: fractional anisotropy; ns: not significant; RD: radial diffusivity; UCMSC: umbilical cord-derived mesenchymal stem cell.

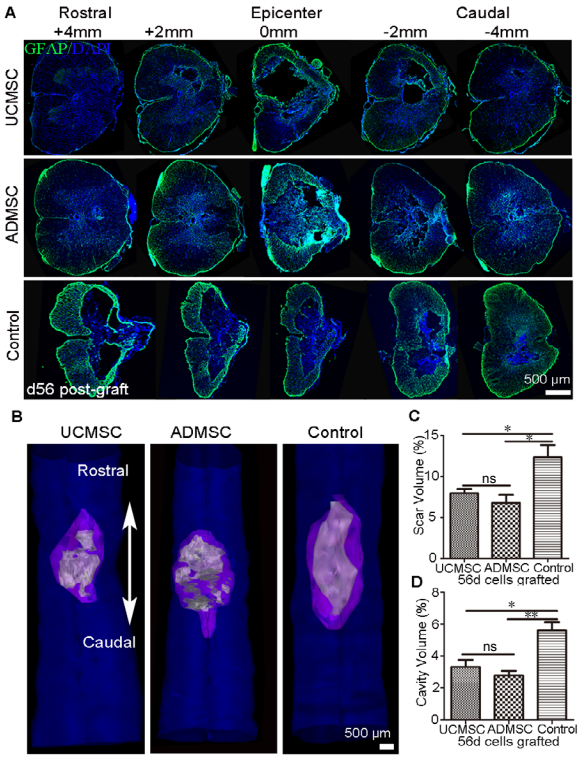

Figure 5 Effects of cell transplantation on glial scar formation and lesion cavity.

(A) Anti-GFAP and DAPI staining indicated glial scar and lesion cavity at different distances from injury sites 56 days (d56) after UCMSC or ADMSC transplantation, and in controls. (B–D) Three-dimensional reconstruction of serial transverse sections within 1 cm spinal cords at d56 after UCMSC or ADMSC transplantation. Both the glial scar (C) and cavity (D) volumes were significantly decreased in UCMSC and ADMSC groups compared with the control group. Data are presented as mean ± SEM (n = 5 per group). *P < 0.05, **P < 0.01 (one-way analysis of variance with Tukey's multiple comparison test). Scale bars: 500 μm. All sections were stained with DAPI (blue). GFAP (green): Alexa Fluor 488. ADMSC: Adipose-derived mesenchymal stem cell; DAPI: 4′,6-diamidino-2-phenylindole; GFAP: glial fibrillary acidic protein; ns: not significant; UCMSC: umbilical cord-derived mesenchymal stem cell.

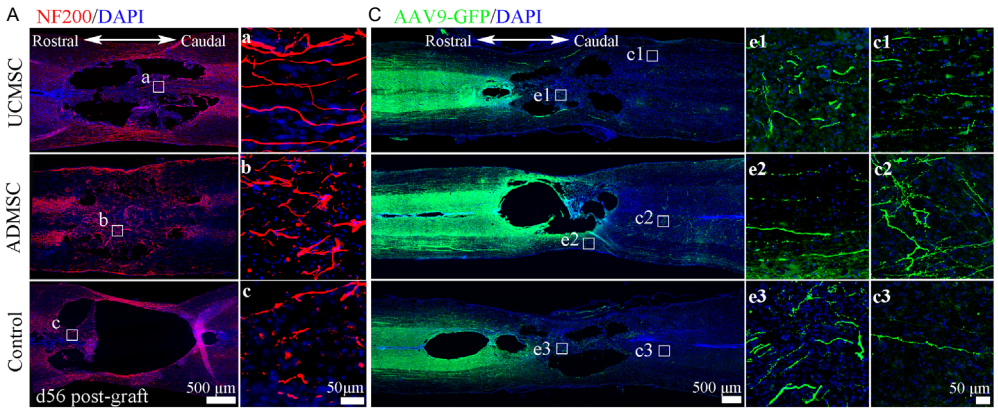

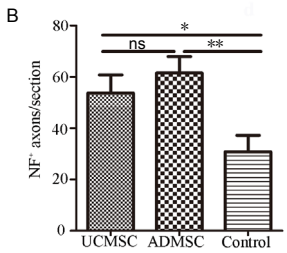

Figure 6 Transplanted cells decrease axon degeneration and promote sprouting.

(A) Anti-NF200 staining of horizontal sections spanning injury epicenters at 56 days (d56) after UCMSC or ADMSC transplantation. Right panels show high magnifications of boxed areas in corresponding left panels. (B) Numbers of neurofilament-positive fibers were significantly higher in UCMSC and ADMSC groups compared with the control group. (C) AAV9-GFP injection at two segments above the injury epicenter (on d42) labeled spared axons at d56 after UCMSC or ADMSC transplantation. Panels e1–3 and c1–3 show high magnification of boxed regions in left panels, representing injury epicenters and caudal spinal cords. (D) GFP-positive fibers were significantly increased at –3 mm of injury epicenters in UCMSC and ADMSC groups compared with the control group. More GFP-positive axons were present in caudal regions than at the injury epicenter. Data are presented as mean ± SEM (n = 6 per group). *P < 0.05, **P < 0.01 (one-way analysis of variance with Tukey's multiple comparison test in B; two-way repeated measures analysis of variance with Bonferroni's *post hoc* correction in D). Scale bars: 500 μm and 50 μm (high magnification regions). All sections are stained with DAPI (blue). NF200 (red): Alexa Fluor 546, AAV9-GFP (green): Alexa Fluor 488. AAV: Adeno-associated virus; ADMSC: adipose-derived mesenchymal stem cell; DAPI: 4′,6-diamidino-2-phenylindole; GFP: green fluorescent protein; NF200: neurofilament 200; ns: not significant; UCMSC: umbilical cord-derived mesenchymal stem cell.

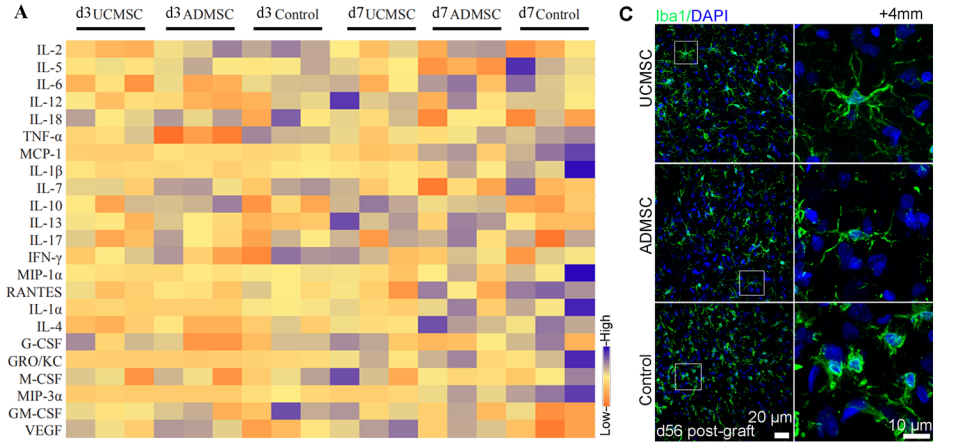

Figure 7 UCMSCs and ADMSCs induce similar modifications of cytokine expression and microglia activation.
(A) Cytokine levels in spinal samples at 3 days (d3) and 7 days (d7) after transplantation, measured using Bio-Plex. (B) In UCMSC and ADMSC groups at d3, upregulation of IL-10 and downregulation of TNF-α was observed only in the ADSMC group, whereas downregulation of MIP-3α was observed in both UCMSC and ADMSC groups. At d7, upregulation of IL-10 and IL-13 was observed in both UCMSC and ADMSC groups. (C) Anti-Iba1 staining of sections +4 mm rostral to injury sites at d56 after transplantation. In UCMSC and ADMSC groups, Iba1-positive cells exhibited star-shaped morphologies, in contrast to the morphology of controls exhibiting round soma and few branches. Scale bars are indicated in each row of panels. All sections were stained with DAPI (blue). Iba1 (green): Alexa Fluor 488. (D) Quantification shows significant increases of Iba1-positive cell densities in UCMSC and ADMSC groups compared with the control group. Data are presented as mean ± SEM (n = 3–6 per group). $*P < 0.05$, $**P < 0.01$ (one-way analysis of variance with Tukey's multiple comparison test). ADMSC: Adipose-derived mesenchymal stem cell; DAPI: 4′,6-diamidino-2-phenylindole; G-CSF: granulocyte colony-stimulating factor; GM-CSF: granulocyte-macrophage colony-stimulating factor; GRO/KC: C-X-C motif chemokine ligand 1; Iba1: ionized calcium-binding adapter molecule 1; IFN-γ: interferon-γ; IL: interleukin; MCP-1: monocyte chemotactic protein 1; M-CSF: macrophage colony-stimulating factor; MIP-1α: macrophage inflammatory protein 1α; MIP-3α: macrophage inflammatory protein 3α; ns: not significant; RANTES: regulated upon activation normal T cell expressed and secreted factor; TNF-α: tumor necrosis factor α; UCMSC: umbilical cord-derived mesenchymal stem cell; VEGF: vascular endothelial growth factor.

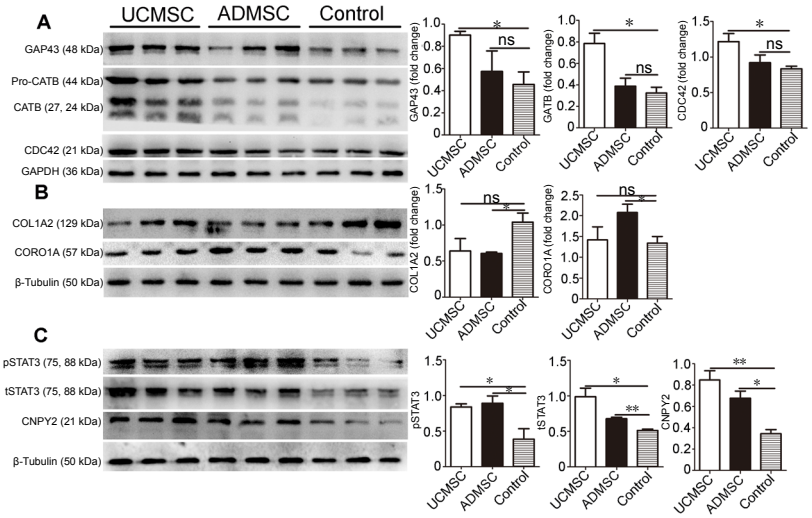

Figure 8 Transplanted cells induce proteomic changes in spinal cord.
(A–C) Western blots to confirm expression of selected proteins. GAP43, CATB, and CDC42 signals were significantly increased in the UCMSC group, but not the ADMSC group (A). There was a significant decrease of COL1A2 and increase of CORO1A in the ADMSC group, but not the UCMSC group (B). Protein level of phosphorylated STAT3 (pSTAT3), total STAT3 (tSTAT3), and CNPY2 were increased in UCMSC and ADMSC groups (C). Data are presented as mean ± SEM (n = 3 animals per group). $*P < 0.05$, $**P < 0.01$ (one-way analysis of variance with Tukey's multiple comparison test). ADMSC: Adipose-derived mesenchymal stem cell; CATB: cathepsin B; CDC42: cell division control protein 42 homolog; CNPY2: canopy 2 homolog (zebrafish); COL1A2: collagen alpha-2 (I) chain; CORO1A: coronin-1A; GAP43: growth associated protein-43; ns: not significant; STAT3: cell division control protein 42 homolog; UCMSC: umbilical cord-derived mesenchymal stem cell.

different effects on axonal regrowth. However, the mechanism by which UCMSCs and ADMSCs regulate endogenous gene expression is unclear. Recent studies showed that MSC-secreted exosomes can invade host cells and regulate gene expression via their microRNA cargo (Xin et al., 2012; Zhang et al., 2017). Thus, differences in exosomes secreted by UCMSCs and ADMSCs might account for their different effects on gene expression.

In conclusion, our comparative study shows that transplanted UCMSCs and ADMSCs similarly contributed to morphological and functional recovery of SCI by fostering anti-neuroinflammatory mechanisms, neural plasticity, and axonal regeneration. However, ADMSCs are a better cell source than UCMSCs for transplantation considering inflammatory modulation during the early period, neurotrophy, and the safety of autologous transplantation. These findings provide a basic knowledge to optimize selection of transplanted cells in clinical settings. Changes in gene expression also provide a readout to dissect the potential mechanisms of transplanted stem cells, which should be studied more extensively in the future.

Acknowledgments: *We wish to thank Ying Wang and Guan-Mao Chen (First Affiliated Hospital of Jinan University, Guangzhou, China) for help with MRI, and the Saliai Stem cell Science and Technology Co., Ltd. (Guangzhou, China) for human ADMSCs.*
Author contributions: *Study concept: LBZ, KFS; study design: LBZ, PPY, AML, YBQ; intellectual content definition: LBZ, AML, PPY, YBQ; literature search: LBZ, AML, PPY; experimental implementation: AML, TL, LTY, LLS; data acquisition: AML, LTY, LLS; data analysis: AML, BLC, LLS; statistical analysis: AML, BLC; manuscript preparation: AML, LBZ; manuscript editing: LBZ, AML, KFS; guarantors: LBZ, KFS. All au-*

thors approved the final version of the paper.

Conflicts of interest: *The authors declare that they have no competing interests.*

Financial support: *This work was supported by Guangdong grant 'Key Technologies for Treatment of Brain Disorders', No. 2018B030332001 (to LBZ); Health and Medical Collaborative Innovation Major Projects of Guangzhou of China, Nos. 201803040016-2 (to LBZ), 201604046028 (to LBZ and KFS); Science & Technology Planning and Key Technology Innovation Projects of Guangdong Province of China, No. 2014B050504006 (to LBZ), Programme of Introducing Talents of Discipline to Universities of China, No. B14036 (to KFS), and Science and Technology Plan Project of Guangdong Province of China, No. 2017B090904033 (to KFS). The funding sources had no role in study conception and design, data analysis or interpretation, paper writing or deciding to submit this paper for publication.*

Institutional review board statement: *Animal experiments were approved by the Laboratory Animal Ethics Committee at Jinan University (approval No. 20180228026) on February 28, 2018, and the application of human stem cells was approved by the Medical Ethics Committee of Medical College of Jinan University of China (approval No. 2016041303) on April 13, 2016.*

Declaration of participant consent: *The authors certify that they have obtained all appropriate forms from the puerpera. In the forms, the puerpera have given their consent for their images and other clinical information to be reported in the journal. The puerpera understand that their names and initials will not be published.*

Biostatistics statement: *The statistical methods of this study were reviewed by the biostatistician of Jinan University of China.*

Copyright license agreement: *The Copyright License Agreement has been signed by all authors before publication.*

Data sharing statement: *Datasets analyzed during the current study are available from the corresponding author on reasonable request.*

Plagiarism check: *Checked twice by iThenticate.*

Peer review: *Externally peer reviewed.*

Additional files:

Additional file 1: *Mesenchymal stem cell culture and identification.*

Additional file 2: *Behavioral tests.*

Additional Table 1: *Primary antibodies list.*

Additional Table 2: *Summary of transplanted cells in the treatment of spinal cord injury.*

Additional Figure 1: *Morphology and characterization of cell lines.*

Additional Figure 2: *UCMSCs and ADMSCs contribute to spinal neuron survival of rats with spinal cord injury after UCMSC and ADMSC transplantation.*

Additional Figure 3: *UCMSC and ADMSC transplantation decreases axon demyelination of rats with spinal cord injury.*

Additional Figure 4: *The expression levels of 23 cytokines after UCMSCs and ADMSCs transplantation in the rats with spinal cord injury.*

Additional Figure 5: *Transplanted cells induce proteins changed related to neurite growth (A), neurotrophin (B), neuroinflammation (C) and apoptosis (D) in the rats with spinal cord injury after UCMSC and ADMSC transplantation.*

References

Abercrombie M (1946) Estimation of nuclear population from microtome sections. Anat Rec 94:239-247.

Amemori T, Jendelová P, Růzicková K, Arboleda D, Syková E (2010) Co-transplantation of olfactory ensheathing glia and mesenchymal stromal cells does not have synergistic effects after spinal cord injury in the rat. Cytotherapy 12:212-225.

Anderson MA, O'Shea TM, Burda JE, Ao Y, Barlatey SL, Bernstein AM, Kim JH, James ND, Rogers A, Kato B, Wollenberg AL, Kawaguchi R, Coppola G, Wang C, Deming TJ, He Z, Courtine G, Sofroniew MV (2018) Required growth facilitators propel axon regeneration across complete spinal cord injury. Nature 561:396-400.

Aung WY, Mar S, Benzinger TL (2013) Diffusion tensor MRI as a biomarker in axonal and myelin damage. Imaging Med 5:427-440.

Bernardo ME, Ball LM, Cometa AM, Roelofs H, Zecca M, Avanzini MA, Bertaina A, Vinti L, Lankester A, Maccario R, Ringden O, Le Blanc K, Egeler RM, Fibbe WE, Locatelli F (2011) Co-infusion of ex vivo-expanded, parental MSCs prevents life-threatening acute GVHD, but does not reduce the risk of graft failure in pediatric patients undergoing allogeneic umbilical cord blood transplantation. Bone Marrow Transplant 46:200-207.

Bhimani AD, Kheirkhah P, Arnone GD, Nahhas CR, Kumar P, Wonais M, Hidrogo H, Aguilar E, Spalinski D, Gopalka M, Roth S, Mehta AI (2017) Functional gait analysis in a spinal contusion rat model. Neurosci Biobehav Rev 83:540-546.

Bianco P, Riminucci M, Gronthos S, Robey PG (2001) Bone marrow stromal stem cells: nature, biology, and potential applications. Stem Cells 19:180-192.

Bornhauser BC, Olsson PA, Lindholm D (2003) MSAP is a novel MIR-interacting protein that enhances neurite outgrowth and increases myosin regulatory light chain. J Biol Chem 278:35412-35420.

Chen S, Zhang W, Wang JM, Duan HT, Kong JH, Wang YX, Dong M, Bi X, Song J (2016) Differentiation of isolated human umbilical cord mesenchymal stem cells into neural stem cells. Int J Ophthalmol 9:41-47.

Choudhery MS, Badowski M, Muise A, Harris DT (2013) Comparison of human mesenchymal stem cells derived from adipose and cord tissue. Cytotherapy 15:330-343.

Dalamagkas K, Tsintou M, Seifalian AM (2018) Stem cells for spinal cord injuries bearing translational potential. Neural Regen Res 13:35-42.

DeBrot A, Yao L (2018) The combination of induced pluripotent stem cells and bioscaffolds holds promise for spinal cord regeneration. Neural Regen Res 13:1677-1684.

Dooley D, Lemmens E, Vangansewinkel T, Le Blon D, Hoornaert C, Ponsaerts P, Hendrix S (2016) Cell-based delivery of interleukin-13 directs alternative activation of macrophages resulting in improved functional outcome after spinal cord injury. Stem Cell Reports 7:1099-1115.

Fernandes M, Valente SG, Sabongi RG, Gomes Dos Santos JB, Leite VM, Ulrich H, Nery AA, da Silva Fernandes MJ (2018) Bone marrow-derived mesenchymal stem cells vs. adipose-derived mesenchymal stem cells for peripheral nerve regeneration. Neural Regen Res 13:100-104.

Gao S, Guo X, Zhao S, Jin Y, Zhou F, Yuan P, Cao L, Wang J, Qiu Y, Sun C, Kang Z, Gao F, Xu W, Hu X, Yang D, Qin Y, Ning K, Shaw PJ, Zhong G, Cheng L, et al. (2019) Differentiation of human adipose-derived stem cells into neuron/motoneuron-like cells for cell replacement therapy of spinal cord injury. Cell Death Dis 10:597.

Gazdic M, Volarevic V, Harrell CR, Fellabaum C, Jovicic N, Arsenijevic N, Stojkovic M (2018) Stem cells therapy for spinal cord injury. Int J Mol Sci 19:1039.

Grant SG, O'Dell TJ, Karl KA, Stein PL, Soriano P, Kandel ER (1992) Impaired long-term potentiation, spatial learning, and hippocampal development in fyn mutant mice. Science 258:1903-1910.

Grasselli G, Strata P (2013) Structural plasticity of climbing fibers and the growth-associated protein GAP-43. Front Neural Circuits 7:25.

Han YF, Tao R, Sun TJ, Chai JK, Xu G, Liu J (2013) Optimization of human umbilical cord mesenchymal stem cell isolation and culture methods. Cytotechnology 65:819-827.

Hausmann ON (2003) Post-traumatic inflammation following spinal cord injury. Spinal Cord 41:369-378.

Hur JW, Cho TH, Park DH, Lee JB, Park JY, Chung YG (2016) Intrathecal transplantation of autologous adipose-derived mesenchymal stem cells for treating spinal cord injury: A human trial. J Spinal Cord Med 39:655-664.

Jain NB, Ayers GD, Peterson EN, Harris MB, Morse L, O'Connor KC, Garshick E (2015) Traumatic spinal cord injury in the United States, 1993-2012. JAMA 313:2236-2243.

Kang E, Burdick KE, Kim JY, Duan X, Guo JU, Sailor KA, Jung DE, Ganesan S, Choi S, Pradhan D, Lu B, Avramopoulos D, Christian K, Mal-hotra AK, Song H, Ming GL (2011) Interaction between FEZ1 and DISC1 in regulation of neuronal development and risk for schizophrenia. Neuron 72:559-571.

Khazaei M, Ahuja CS, Rodgers CE, Chan P, Fehlings MG (2019) Generation of definitive neural progenitor cells from human pluripotent stem cells for transplantation into spinal cord injury. Methods Mol Biol 1919:25-41.

Kim KD, Ament JD (2017) Spinal cord injury treatment: What's on the Horizon? Spine (Phila Pa 1976) 42 Suppl 7:S21.

Lehmann HC, Zhang J, Mori S, Sheikh KA (2010) Diffusion tensor imaging to assess axonal regeneration in peripheral nerves. Exp Neurol 223:238-244.

Li J, Chen S, Zhao Z, Luo Y, Hou Y, Li H, He L, Zhou L, Wu W (2017) Effect of VEGF on inflammatory regulation, neural survival, and func-tional improvement in rats following a complete spinal cord transection. Front Cell Neurosci 11:381.

Matyas JJ, Stewart AN, Goldsmith A, Nan Z, Skeel RL, Rossignol J, Dunbar GL (2017) Effects of bone-marrow-derived MSC transplantation on functional recovery in a rat model of spinal cord injury: comparisons of transplant locations and cell concentrations. Cell Transplant 26:1472-1482.

Mehta ST, Luo X, Park KK, Bixby JL, Lemmon VP (2016) Hyperactivated Stat3 boosts axon regeneration in the CNS. Exp Neurol 280:115-120.

Mukhamedshina YO, Gracheva OA, Mukhutdinova DM, Chelyshev YA, Rizvanov AA (2019) Mesenchymal stem cells and the neuronal microenvironment in the area of spinal cord injury. Neural Regen Res 14:227-237.

Munir H, McGettrick HM (2015) Mesenchymal stem cell therapy for autoimmune disease: risks and rewards. Stem Cells Dev 24:2091-2100.

Nakajima H, Uchida K, Guerrero AR, Watanabe S, Sugita D, Takeura N, Yoshida A, Long G, Wright KT, Johnson WE, Baba H (2012) Trans-plantation of mesenchymal stem cells promotes an alternative pathway of macrophage activation and functional recovery af-ter spinal cord injury. J Neurotrauma 29:1614-1625.

Orlandin JR, Ambrósio CE, Lara VM (2017) Glial scar-modulation as therapeutic tool in spinal cord injury in animal models. Acta Cir Bras 32:168-174.

Pertz OC, Wang Y, Yang F, Wang W, Gay LJ, Gristenko MA, Clauss TR, Anderson DJ, Liu T, Auberry KJ, Camp DG 2nd, Smith RD, Klemke RL (2008) Spatial mapping of the neurite and soma proteomes reveals a functional Cdc42/Rac regulatory network. Proc Natl Acad Sci U S A 105:1931-1936.

Pittenger MF, Mackay AM, Beck SC, Jaiswal RK, Douglas R, Mosca JD, Moorman MA, Simonetti DW, Craig S, Marshak DR (1999) Multilineage potential of adult human mesenchymal stem cells. Science 284:143-147.

Ruzicka J, Machova-Urdzikova L, Gillick J, Amemori T, Romanyuk N, Karova K, Zaviskova K, Dubisova J, Kubinova S, Murali R, Sykova E, Jhanwar-Uniyal M, Jendelova P (2017) A comparative study of three different types of stem cells for treatment of rat spinal cord injury. Cell Transplant 26:585-603.

Salewski RP, Mitchell RA, Li L, Shen C, Milekovskaia M, Nagy A, Fehlings MG (2015) Transplantation of induced pluripotent stem cell-derived neural stem cells mediate functional recovery following thoracic spinal cord injury through remyelination of axons. Stem Cells Transl Med 4:743-754.

Secco M, Zucconi E, Vieira NM, Fogaça LL, Cerqueira A, Carvalho MD, Jazedje T, Okamoto OK, Muotri AR, Zatz M (2008) Multipotent stem cells from umbilical cord: cord is richer than blood! Stem Cells 26:146-150.

Shin E, Kashiwagi Y, Kuriu T, Iwasaki H, Tanaka T, Koizumi H, Gleeson JG, Okabe S (2013) Doublecortin-like kinase enhances dendritic remodelling and negatively regulates synapse maturation. Nat Commun 4:1440.

Sun G, Yang S, Cao G, Wang Q, Hao J, Wen Q, Li Z, So KF, Liu Z, Zhou S, Zhao Y, Yang H, Zhou L, Yin Z (2018) γδ T cells provide the early source of IFN-γ to aggravate lesions in spinal cord injury. J Exp Med 215:521-535.

Suo D, Park J, Harrington AW, Zweifel LS, Mihalas S, Deppmann CD (2014) Coronin-1 is a neurotrophin endosomal effector that is required for developmental competition for survival. Nat Neurosci 17:36-45.

Tang Q, Zhang C, Wu X, Duan W, Weng W, Feng J, Mao Q, Chen S, Jiang J, Gao G (2018) Comprehensive proteomic profiling of patients' tears identifies potential biomarkers for the traumatic vegetative state. Neurosci Bull 34:626-638.

Thompson CD, Zurko JC, Hanna BF, Hellenbrand DJ, Hanna A (2013) The therapeutic role of interleukin-10 after spinal cord injury. J Neurotrauma 30:1311-1324.

Torres-Espín A, Corona-Quintanilla DL, Forés J, Allodi I, González F, Udina E, Navarro X (2013) Neuroprotection and axonal regeneration after lumbar ventral root avulsion by re-implantation and mesenchymal stem cells transplant combined therapy. Neurotherapeutics 10:354-368.

Tran AP, Sundar S, Yu M, Lang BT, Silver J (2018) Modulation of receptor protein tyrosine phosphatase sigma increases chondroitin sulfate proteoglycan degradation through cathepsin B secretion to enhance axon outgrowth. J Neurosci 38:5399-5414.

Vaquero J, Zurita M, Rico MA, Bonilla C, Aguayo C, Montilla J, Bustamante S, Carballido J, Marin E, Martinez F, Parajon A, Fernandez C, Reina L (2016) An approach to personalized cell therapy in chronic complete paraplegia: The Puerta de Hierro phase I/II clinical trial. Cytotherapy 18:1025-1036.

Wang L, Wei FX, Cen JS, Ping SN, Li ZQ, Chen NN, Cui SB, Wan Y, Liu SY (2014) Early administration of tumor necrosis factor-alpha antagonist promotes survival of transplanted neural stem cells and axon myelination after spinal cord injury in rats. Brain Res 1575:87-100.

Wu X, Zhang YP, Qu W, Shields LBE, Shields CB, Xu XM (2017) A tissue displacement-based contusive spinal cord injury model in mice. J Vis Exp:54988.

Xin H, Li Y, Buller B, Katakowski M, Zhang Y, Wang X, Shang X, Zhang ZG, Chopp M (2012) Exosome-mediated transfer of miR-133b from multipotent mesenchymal stromal cells to neural cells contributes to neurite outgrowth. Stem Cells 30:1556-1564.

Yang Z, Zhang A, Duan H, Zhang S, Hao P, Ye K, Sun YE, Li X (2015) NT3-chitosan elicits robust endogenous neurogenesis to enable func-tional recovery after spinal cord injury. Proc Natl Acad Sci U S A 112:13354-13359.

Zhang W, Yang B, Weng H, Liu T, Shi L, Yu P, So KF, Qu Y, Zhou L (2019) Wheel running improves motor function and spinal cord plasticity in mice with genetic absence of the corticospinal tract. Front Cell Neurosci 13:106.

Zhang Y, Chopp M, Liu XS, Katakowski M, Wang X, Tian X, Wu D, Zhang ZG (2017) Exosomes derived from mesenchymal stromal cells promote axonal growth of cortical neurons. Mol Neurobiol 54:2659-2673.

Zhou Z, Chen Y, Zhang H, Min S, Yu B, He B, Jin A (2013) Comparison of mesenchymal stromal cells from human bone marrow and adi-pose tissue for the treatment of spinal cord injury. Cytotherapy 15:434-448.

C-Editor: Zhao M; S-Editors: Yu J, Li CH; L-Editors: Dausen AV, Yu J, Song CP; T-Editor: Jia Y

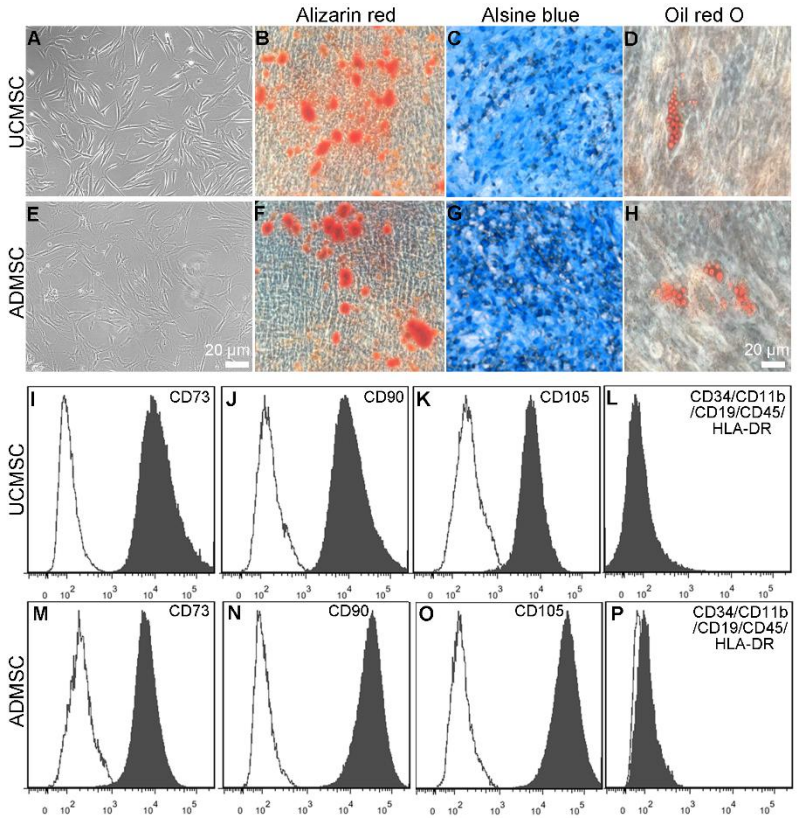

Additional Figure 1 Morphology and characterization of cell lines.

(A–D) At 4th passage, umbilical cord-derived mesenchymal stem cells (UCMSCs) have long spindle shapes when viewed in phase contrast (A), and can differentiate into osteocytes, chondrocytes and adipocytes, as shown by alizarin red (B), alcian blue staining (C) and oil red O (D) staining, respectively. (E–H) A similar morphology (E) and differentiation potential assessed is found in passage-4 generation of adipose-derived mesenchymal stem cells (ADMSCs). (I–P) Flow cytometry analysis show that more than 95% of UCMSCs (I-L) and ADMSCs (M-P) are positive for CD73 (I, M), CD90 (J, N) and CD105 (K, O), typical mesenchymal stem cell markers, and less than 2% of them are positive for CD34, CD11b, CD19, CD45 and HLA-DR (L, P), mesenchymal stem cell-negative makers, indicating cells at high purity for transplantation. Scale bars: 20 μm.

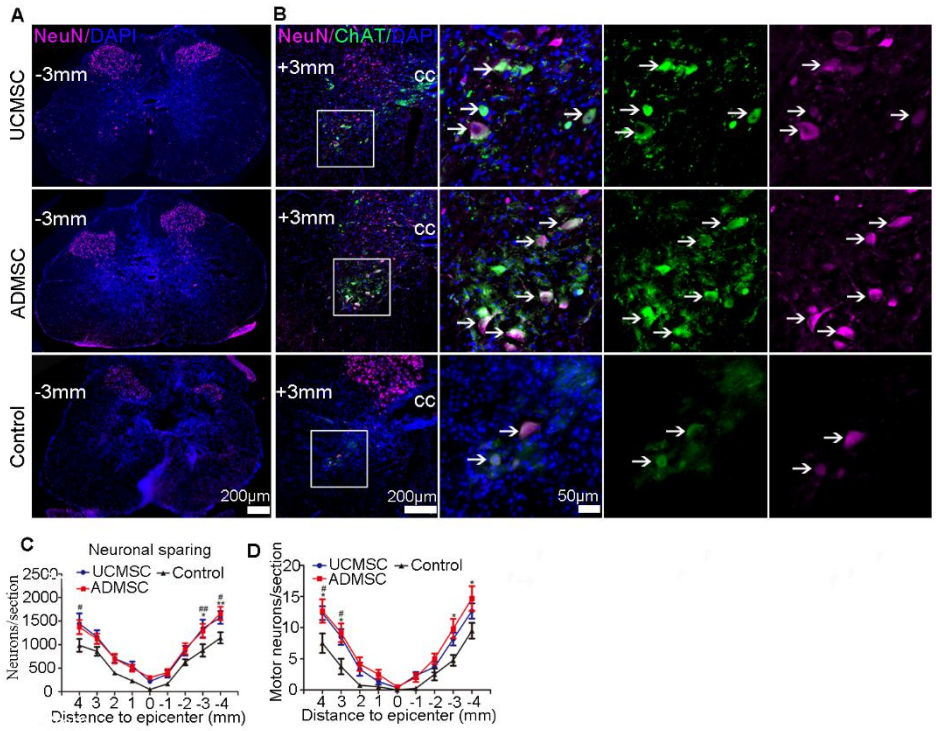

Additional Figure 2 UCMSCs and ADMSCs contribute to spinal neuron survival of rats with spinal cord injury after UCMSC and ADMSC transplantation.

(A) Anti-NeuN staining of spinal sections caudal (-3 mm) from injury site, 56 days after transplantation. (B) ChAT (green) and NeuN (violet) double immunofluorescent staining in spinal sections +3 mm from the injury 56 days after UCMSCs or ADMSCs transplantation. All ChAT-positive neurons co-express NeuN (arrows). Blue: DAPI. Right panels are close-ups of areas boxed in left panels. Scale bars: 200 μm in A, B, 50 μm in the other columns of B. (C) Quantification of NeuN-positive cells at different levels from injury. NeuN positive cells in the UCMSC and ADMSC groups +4 mm, -3 mm and -4 mm from the epicenter in UCMSC and ADMSC groups were more than those in control group. (D) More ChAT-positive neurons are seen in the UCMSC and ADMSC groups in segments +4 mm, +3 mm, -3 mm and -4 mm from the epicenter than those in control group. Data were expressed as the mean ± SEM (n = 6 in each group). UCMSC *versus* control: #P < 0.05; ##P < 0.01. ADMSC *versus* control: *P < 0.05; **P < 0.01. Two-way repeated measures analysis of variance with Bonferroni's *post hoc* correction. ADMSCs: Adipose-derived mesenchymal stem cells; cc: central canal; ChAT: choline acetyltransferase; DAPI: 4',6-diamidino-2-phenylindole; UCMSCs: umbilical cord-derived mesenchymal stem cells. NeuN (violet): Alexa Fluor 546, ChAT (green): Alexa Fluor 488.

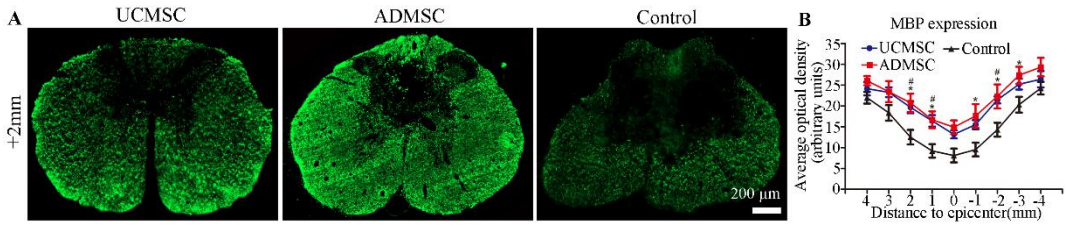

Additional Figure 3 UCMSC and ADMSC transplantation decreases axon demyelination of rats with spinal cord injury.

(A, B) Anti-MBP staining of transverse spinal cord sections 56 days after transplantation. In sections +2 mm rostral to injury epicenter, MBP immunoreactivity is stronger in the UCMSC and ADMSC groups than that in the control group (A). Scale bar: 200 μm. Quantification shows significant increase of MBP-immunoreactive density in sections spanning injury epicenters, from rostral +2 mm to caudal -3 mm level, in the UCMSC and ADMSC groups compared to the control group (B). Data were expressed as the mean ± SEM (n = 6 in each group), and analyzed by two-way repeated measures analysis of variance with Bonferroni's *post hoc* correction. #P < 0.05, UCMSC *versus* control; *P < 0.05, ADMSC *versus* control. ADMSCs: Adipose-derived mesenchymal stem cells; MBP: myelin basic protein; UCMSCs: umbilical cord-derived mesenchymal stem cells. MBP (green): Alexa Fluor 488.

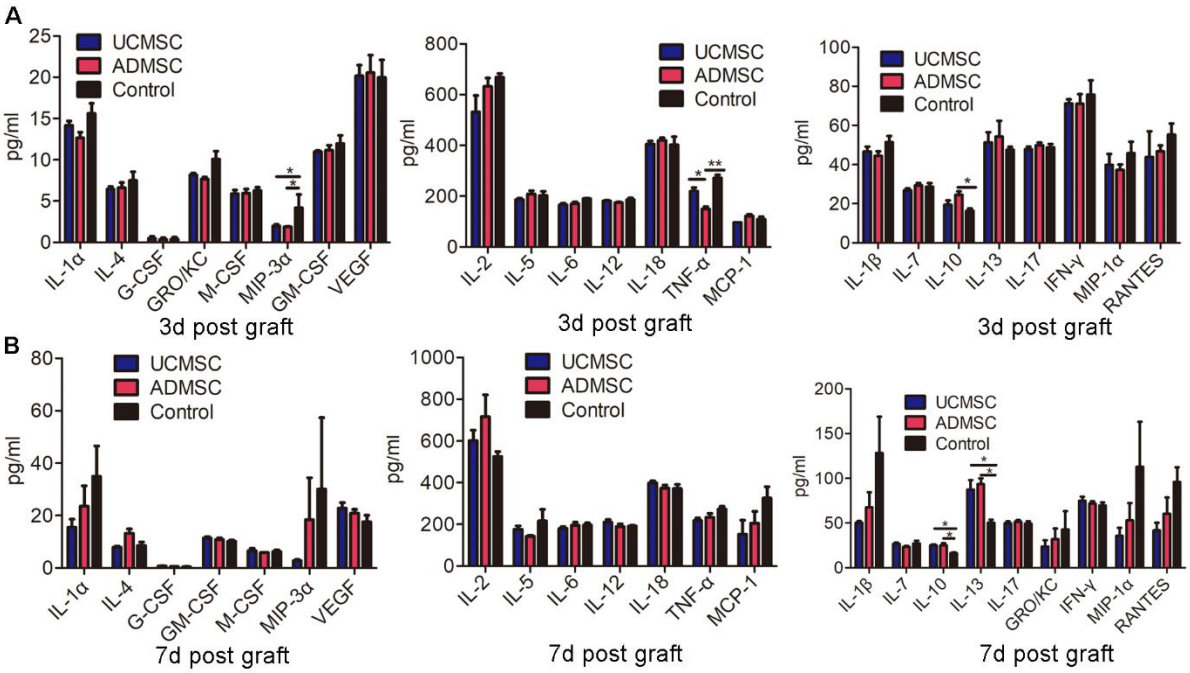

Additional Figure 4 The expression levels of 23 cytokines after UCMSCs and ADMSCs transplantation in the rats with spinal cord injury.

(A, B) Expression level of 23 cytokines in spinal samples 3 (A) and 7 (B) days after cells transplantation. Data were expressed as the mean ± SEM (n = 3 in each group).*P < 0.05, **P < 0.01 (one-way analysis of variance with Tukey's multiple comparison test). ADMSCs: Adipose-derived mesenchymal stem cells; G-CSF: granulocyte colony-stimulating factor; GM-CSF: granulocyte-macrophage colony-stimulating factor; GRO/KC: C-X-C motif chemokine ligand 1; IFN-γ: interferon-γ; IL: interleukin; MCP-1: monocyte chemotactic protein 1; M-CSF: macrophage colony-stimulating factor; MIP-1α: macrophage inflammatory protein 1α; MIP-3α: macrophage inflammatory protein 3α; RANTES: regulated upon activation normal T cell expressed and secreted factor; TNF-α: tumor necrosis factor α; UCMSCs: umbilical cord-derived mesenchymal stem cells; VEGF: Vascular endothelial growth factor.

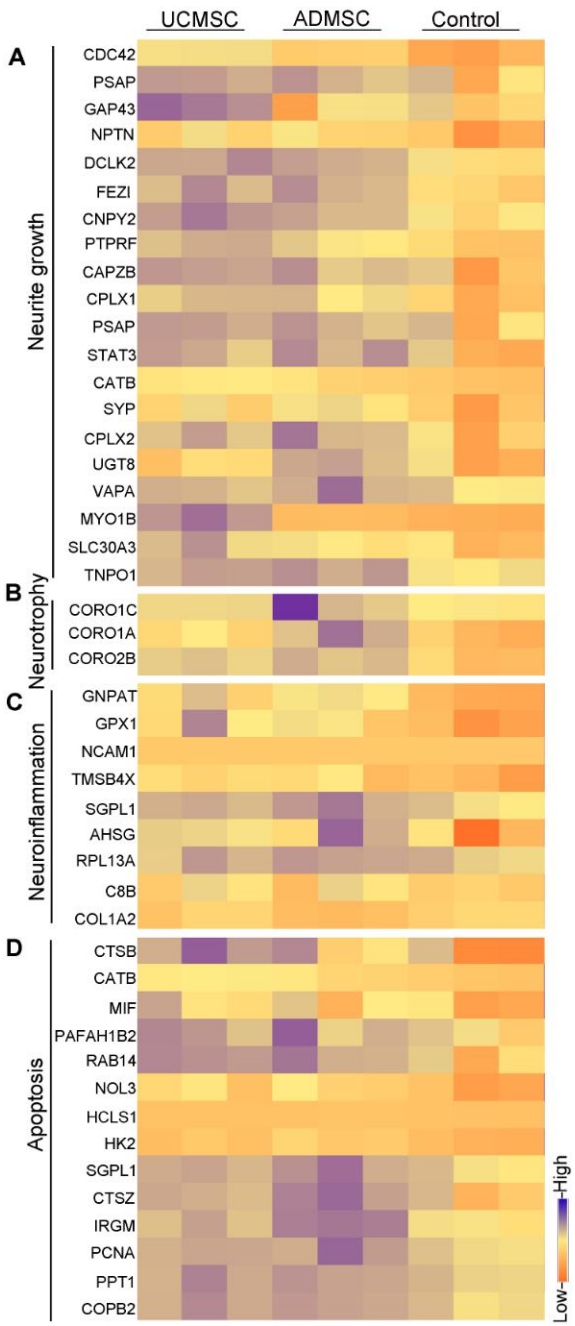

Additional Figure 5 Transplanted cells induce proteins changed related to neurite growth (A), neurotrophin (B), neuroinflammation (C) and apoptosis (D) in the rats with spinal cord injury at 7 days after UCMSC and ADMSC transplantation.

The color from orange to blue presents the cytokine concentration from low to high. ADMSC: Adipose-derived mesenchymal stem cell; AHSG: α-2-HS-glycoprotein; CAPZB: capping actin protein of muscle Z-line subunit β; CATB: cathepsin B; CDC42: cell division control protein 42 homolog; CNPY2: canopy 2 homolog (Zebrafish); COPB2: copper resistance protein B; CORO1A: coronin-1A; CORO1C: coronin-1C; CORO2B: coronin-2B; CPLX1: complexin-1; CPLX2: complexin-2; CTSB: cathepsin B; CTSZ: Cathepsin Z; DCLK3: serine/threonine-protein kinase DCLK3; FEZI: fasciculation and elongation protein zeta-1; GAP43: growth associated protein-43; GNPAT: glyceronephosphate O-acyltransferase; GPX1: glutathione peroxidase 1; HCLS1: hematopoietic lineage cell-specific protein 1; HK2: hexokinase 2; IRGM: immunity related GTPase M; MIF: macrophage migration inhibitory factor; MYO1B: unconventional myosin-1b; NCAM1: neural cell adhesion molecule 1; NOL3: nucleolar protein 3; NPTN: neuroplastin; PAFAH1B2: platelet activating factor acetylhydrolase 1b catalytic subunit 2; PPT1: palmitoyl-protein thioesterase 1; PSAP: prosaposin; PTPRF: receptor-type tyrosine-protein phosphatase F; PCNA: proliferating cell nuclear antigen; RAB14: Ras-related protein 14; RPL13A: ribosomal protein L13a; SGPL1: sphingosine-1-phosphate lyase 1; SLC30A3: zinc transporter 3; STAT3: signal transducer and activator of transcription 3; SYP: synaptophysin; TMSB4X: thymosin β4 X-linked; TNPO1: transportin 1; UCMSC: umbilical cord-derived mesenchymal stem cell; UGT8: glycosyltransferase 8; VAPA: vesicle-associated membrane protein-associated protein A.

Additional Table 1 Primary antibodies list

Antibody	Source	Dilution	Catalog number	Company	Method
tStat3	Rabbit	1:1000	ab68153	Abcam	WB
GAP43	Rabbit	1:1000	ab75810	Abcam	WB
CDC42	Rabbit	1:1000	ab187643	Abcam	WB
pStat3	Rabbit	1:1000	ab76315	Abcam	WB
COL1A2	Rabbit	1:1000	ab96723	Abcam	WB
CATB	Rabbit	1:1000	31718	Cell Signaling Tech	WB
CNPY2	Rabbit	1:1000	14635-1-AP	Proteintech	WB
CORO1A	Rabbit	1:1000	SAB4200078	Sigma	WB
GAPDH	Mouse	1:5000	ab8245	Abcam	WB
β-Tubulin	Rabbit	1:5000	ab6046	Abcam	WB
HUNA	Mouse	1:1000	mab1281	Millipore	IF
GFAP	Rat	1:1000	13-0300	Thermo Fisher	IF
TUJ1	Rabbit	1:1000	ab18207	Abcam	IF
NeuN	Mouse	1:1000	ab104224	Abcam	IF
PAX6	Mouse	1:500	Ab5790	Abcam	IF
Olig2	Rabbit	1:1000	ab6910	Abcam	IF
MBP	Rabbit	1:1000	m3821	Sigma	IF
ChAT	Goat	1:500	AB144P	Millipore	IF
Iba1	Rabbit	1:1000	019-19741	Wako	IF
NF-200	Rabbit	1:1000	ab40796	Abcam	IF

CATB: cathepsin B; CDC42: cell division control protein 42 homolog; ChAT: choline acetyltransferase; CNPY2: canopy 2 homolog (Zebrafish); COL1A2: collagen alpha-2(I) chain; CORO1A: coronin-1A; GAP43: growth associated protein-43; GAPDH: glyceraldehyde-3-phosphate dehydrogenase; GFAP: glial fibrillary acidic protein; HUNA: human nuclear antigen; Iba1: ionized calcium-binding adapter molecule 1; IF: immunofluorescence; MBP: myelin basic protein; NF-200: neurofilament 200; PAX6: paired box 6; pSTAT3: phosphorylated signal transducer and activator of transcription 3; tSTAT3: total signal transducer and activator of transcription 3; TUJ1: βIII-tubulin; WB: western blot assay.

Additional Table 2 Summary of transplanted cells in the treatment of spinal cord injury

Cells	Survival	Differentiation	Function	Microenvironment	Mechanisms
Umbilical cord-derived mesenchymal stem cells	~4 weeks	No	Motor: ↑; Sensory: ↑; Motor-evoked potential: ↑	Neuron: ↑; Fiber: ↑; Myelin: ↑; Lesion volume: ↓; Glial scar: ↓; Active macrophages: ↓	Anti-inflammation: ↑; Neurotrophy: ?; Axonal growth: ↑↑
Adipose-derived mesenchymal stem cells	~4 weeks	No	Motor: ↑; Sensory: ↑; Motor-evoked potential: ↑	Neuron: ↑; Fiber: ↑; Myelin: ↑; Lesion volume: ↓; Glial scar: ↓; Active macrophages: ↓	Anti-inflammation: ↑↑; Neurotrophy: ↑↑; Axonal growth: ↑

"↑": Improving or increasing; "↓": decreasing; "?": not clear.